ChemComm

COMMUNICATION

View Article Online
View Journal | View Issue

Cite this: *Chem. Commun.*, 2022, **58**, 8396

Received 21st April 2022,
Accepted 1st June 2022

DOI: 10.1039/d2cc02272a

rsc.li/chemcomm

Electrocatalytic activity for proton reduction by a covalent non-metal graphene–fullerene hybrid†

Demetrios D. Chronopoulos, ‡[a] Christina Stangel,‡[b] Magdalena Scheibe,[a] Klára Čépe,[a] Nikos Tagmatarchis *[b] and Michal Otyepka *[ac]

A non-metal covalent hybrid of fullerene and graphene was synthesized in one step *via* fluorographene chemistry. Its electrocatalytic performance for the hydrogen evolution reaction and durability was ascribed to intrahybrid charge-transfer phenomena, exploiting the electron-accepting properties of C_{60} and the high conductivity and large surface area of graphene.

Electrocatalytic water splitting into oxygen and hydrogen is one of the most promising processes for the sustainable production of hydrogen as a carbon-neutral fuel.[1] The most effective electrocatalysts, which are commercially used in water electrolysis devices and fuel cells, are based on Pt and RuO_2.[2] The prohibitive scarcity and cost of the noble metals limit the future development of a hydrogen-based economy. Owing to their low price and earth abundance, non-precious metal-based electrocatalysts, mainly composed of transition metals, are employed as alternatives.[3] However, all metal-based catalysts face challenges such as low selectivity, poor durability, agglomeration and environmental issues.[4] Therefore, it is necessary to develop efficient, low cost and highly durable catalysts of the hydrogen evolution reaction (HER) to support the growth of the hydrogen economy.[5–7] Besides efforts toward minimizing the HER overpotential, and increasing the reaction kinetics, catalyst electrical conductivity and stability,[8,9] a new class of catalysts composed of lightweight and abundant elements must be developed. Towards this end, the development of carbon-based metal-free electrocatalysts has been launched, receiving remarkable attention.[4]

Remarkable electron acceptor properties of fullerenes have rendered them as great candidates for the synthesis of efficient multifunctional metal-free electrocatalysts.[10] Heterostructures based on fullerene (mainly C_{60}) and low dimensional nanomaterials are gaining increasing interest due to their unique physicochemical properties, such as large surface areas and great electronic and mechanical properties.[11] These heterostructures appear as efficient noble-metal-free and low-cost electrocatalysts to compete with precious state-of-the-art noble-metal catalysts.[12] Noticeably, a non-metal carbon-based electrocatalyst was prepared through the adsorption of C_{60} onto single-walled carbon nanotubes (SWCNTs), which exhibited excellent performance toward the HER, oxygen evolution reaction (OER) and oxygen reduction reaction (ORR). Evidently, intermolecular charge transfer between C_{60} and SWCNTs largely induced high electrocatalytic activities.[13] Additionally, a bimetallic phosphide Ni–Co–P coupled with C_{60} presented excellent HER activity, and it was concluded that C_{60} improved the electrocatalytic activity for the HER by enhancing the surface roughness and electrical conductivity.[14] In another study, a covalently linked graphene–C_{60} hybrid, which was prepared *via* ball-milling, was employed as an electrocatalyst toward the ORR,[15] exhibiting higher catalytic activity than that of the individual species C_{60} and graphite. This finding was ascribed to the generation of a positively charged graphene basal plane, as a result of charge transfer to C_{60}. Also, covalently linked CNT–C_{60} hybrids very efficiently catalyze the two-electron reduction of oxygen to H_2O_2 due to high electron mobility through the fullerene units, large surface area and covalent linkage between C_{60} and CNTs.[16] Nevertheless, the use of C_{60} as a potential electrocatalyst is rare; hence, it is of greatest interest to further investigate its covalent conjugation onto graphene and scrutinize the electrocatalytic performance of the newly formed heterostructure for proton reduction toward hydrogen evolution.

In recent years, fluorographene (FG)[17,18] has been employed as an effective precursor for the preparation of covalently modified graphene derivatives with high conductivity and

[a] *Regional Centre of Advanced Technologies and Materials, Czech Advanced Technology and Research Institute (CATRIN), Palacký University Olomouc, Šlechtitelů 27, Olomouc 779 00, Czech Republic. E-mail: michal.otyepka@upol.cz*
[b] *Theoretical and Physical Chemistry Institute, National Hellenic Research Foundation, 48 Vassileos Constantinou Avenue, Athens 11635, Greece. E-mail: tagmatar@eie.gr*
[c] *IT4Innovations, VSB – Technical University of Ostrava, 17. listopadu 2172/15, 708 00 Ostrava-Poruba, Czech Republic*

† Electronic supplementary information (ESI) available. See DOI: https://doi.org/10.1039/d2cc02272a

‡ Both authors contributed equally.

functionalization degree,[19,20] synthesizing metal-free electrocatalysts for the ORR as well.[21–23] However, graphene derivatives produced by FG have not been studied in other electrocatalytic reactions. Moreover, from the synthetic point of view, the utilization of FG as a template for the hybridization with C_{60} has not been reported yet. Strikingly, the efficient intermolecular charge-transfer processes between graphene derivatives and fullerene nanocages are expected to result in a large number of active sites, which may favor electrocatalytic processes.

Herein, we exploited the high conductivity and large surface area of graphene derivatives produced by FGs with excellent electron acceptor properties of C_{60} to prepare a novel carbon-based, metal-free electrocatalyst for the HER. In this frame, a covalently linked graphene–fullerene hybrid (denoted as G–C_{60} henceforth) was synthesized *via* the chemistry of FGs and characterized by complementary spectroscopic, microscopy, and thermal analysis techniques. Additionally, the electrocatalytic activity of G–C_{60} for the HER was studied for the first time by performing linear sweep voltammetry (LSV) measurements and electrochemical impedance spectroscopy (EIS), showing significantly improved electrocatalytic activity in comparison with its precursors. The synergistic interactions between the formed graphene by FG and C_{60} promoted the formation of abundant active sites for electrocatalytic proton reduction.

Compounds bearing amino groups are widely employed as nucleophiles for the efficient covalent modification of FG. Thus, a fulleropyrrolidine derivative carrying a primary amino moiety as a nucleophile (C_{60}-pyr-NH_2)[24] reacted with the electrophilic FG (Fig. 1).[25] The reaction was conducted at 130 °C in dry 1,2-dichlorobenzene (*o*-DCB) under a nitrogen atmosphere. Owing to the cascade substitution and defluorination, G–C_{60} was successfully synthesized. The inertness of C_{60} to cause reductive defluorination in FG was also studied through a control experiment (see Section S1.3 and Fig. S1 in the ESI†).

Successful covalent linking of fullerene derivative C_{60}-pyr-NH_2 onto the graphene lattice was proved by Fourier-transform infrared (FT-IR) spectroscopy (Fig. 2(A)). The FT-IR spectrum of the G–C_{60} hybrid displayed the aliphatic C–H stretching vibrations of the ethylene glycol chain at 2980–2850 cm^{-1} and characteristic vibrational peaks attributed to C_{60} at 1450, 1130 and 525 cm^{-1}.[26] Moreover, the significant reduction of the ascribed peak to the C–F bonds at 1200 cm^{-1} and the appearance of two bands at around 1585 and 1460 cm^{-1} verified the formation of the conjugated C=C double bonds due to the reductive defluorination of FG,[27] which occurs simultaneously with the covalent grafting of fullerene derivative C_{60}-pyr-NH_2.

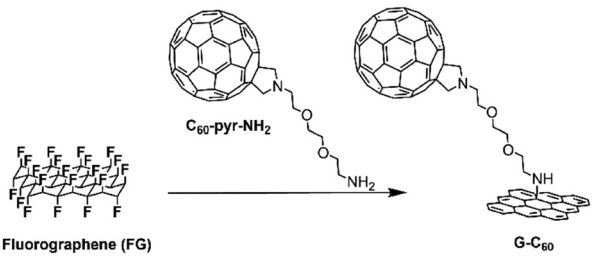

Fig. 1 Preparation of the G–C_{60} hybrid *via* the chemistry of fluorographene.

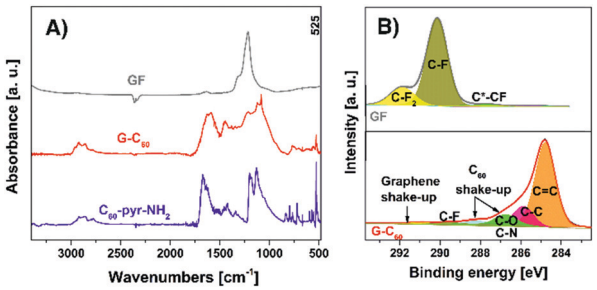

Fig. 2 (A) FT-IR spectra of pristine GF, C_{60}-pyr-NH_2 and G–C_{60}, and (B) HR-XPS C 1s spectra of pristine GF (upper panel) and G–C_{60} (lower panel).

X-ray photoelectron spectroscopy (XPS) measurements also confirmed the successful synthesis of G–C_{60} providing information about the chemical composition of the material. According to atomic content analyses obtained from XPS, G–C_{60} showed an almost quantitative elimination of fluorine atoms (1.5 at% of F) in G–C_{60} with respect to 55.7 at% in graphite fluoride (GF) (Fig. S2 and Table S1, ESI†). In this context, the high-resolution C 1s XPS spectrum of G–C_{60} corroborated the nucleophilic substitution and reductive defluorination of FG, since the intensity of the C–F_x components at 288–293 eV practically disappeared (Fig. 2(B)). On the other hand, new bands appeared at 284.8 and 285.8 eV, ascribed to sp^2 and sp^3 carbons, respectively, indicating the formation of a graphenic network and the covalent linking of C_{60}-pyr-NH_2.[28] Moreover, a peak attributed to nitrogen appeared at around 400 eV, due to its presence in the fullerene derivative (Fig. S2, ESI†).

Raman spectroscopy provided further proof of the FG reduction due to the nucleophilic substitution and the formation of the G–C_{60} hybrid (Fig. S3, ESI†). Whereas the precursor GF is Raman inactive,[29] the Raman spectrum of the hybrid exhibited the characteristic D and G bands at around 1330 and 1600 cm^{-1}, respectively, demonstrating the construction of a graphene lattice through the formation of sp^2 lattice-carbons (G-band) and the conjugation of C_{60}-pyr-NH_2 units through the formation of sp^3 hybridized carbons (D-band). The intensity ratio (I_D/I_G) was found to be 1.29, as also observed for other graphene derivatives prepared *via* the chemistry of FG.[19]

Thermogravimetric analysis (TGA) was employed under a nitrogen atmosphere to assess the thermal stability and degree of functionalization of the hybrid (Fig. S4, ESI†). The pristine GF is thermally stable below 400 °C and decomposes in the temperature range of 450–650 °C, losing 75% of its weight.[29] On the other hand, decomposition of G–C_{60} started at 175 °C and completed at 600 °C, exhibiting a weight loss of ~30% of the initial mass. Importantly, C_{60}-pyr-NH_2 started decomposing at a lower temperature (155 °C). According to the thermographs of these materials, the higher thermal stability of the fullerene unit on G–C_{60} can be ascribed to its covalent conjugation with the graphene lattice.

Additionally, the redox properties of G–C_{60} were assessed in *o*-DCB and 0.1 M $TBAPF_6$ as electrolyte *vs.* Fc/Fc^+ with the aid of

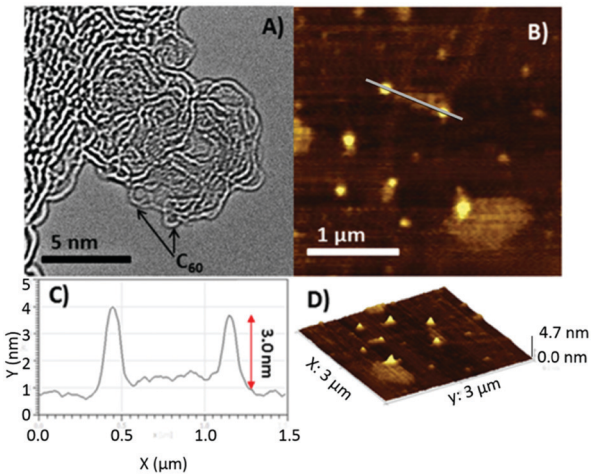

Fig. 3 (A) HR-TEM, and (B)–(D) AFM images and height profile of G–C_{60}.

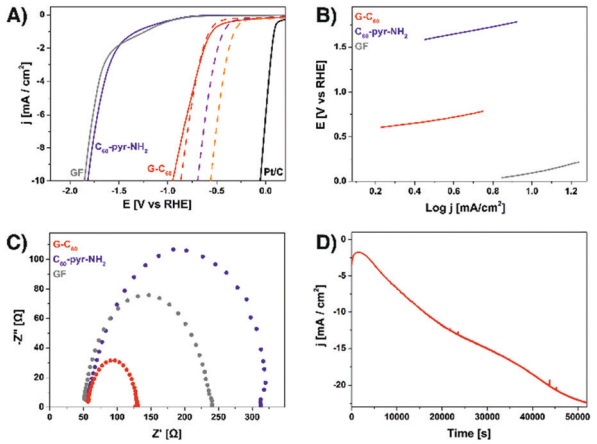

Fig. 4 (A) Polarization curves for the HER of benchmark Pt/C (black line), GF (grey), C_{60}-pyr-NH_2 (blue line), and G–C_{60} before (red line) and after 1000 (dashed red line), 5000 (dashed purple line) and 10 000 (dashed orange line) cycles respectively, (B) Tafel slopes, and (C) Nyquist plots of GF (grey), C_{60}-pyr-NH_2 (blue) and G–C_{60} (red), and (D) chronoamperometric response of G–C_{60} (red), at an applied potential of −1.86 V.

differential pulse voltammetry (Fig. S5, ESI†). The corresponding differential pulse voltammogram is compared with that acquired from C_{60}-pyr-NH_2. In short, C_{60}-pyr-NH_2 exhibited three reversible reductions at −1.30, −1.67, and −2.22 V.[30,31] Concerning G–C_{60}, the reversible reduction at −2.22 V seems to have been shifted to −1.87 V, implying the existence of interactions between both components.[31,32] However, the other two reductions are not clearly observed, specifically the reversible peak at −1.67 V appeared broadened.

The morphology of G–C_{60} was explored by high resolution transmission electron microscopy (HR-TEM) and atomic force microscopy (AFM) (Fig. 3(A)–(D)). A representative HR-TEM image of G–C_{60} indicated the hybridization of FG with C_{60}-pyr-NH_2. According to Fig. 3(A), spherical species, having a diameter of around 0.8 nm, are linked with graphene layers at their edges. The AFM analysis (Fig. 3(B)–(D)) showed that the height of G–C_{60} was around 3.0 nm, which corresponded well to the thickness of the hybrid material.

Finally, the electrocatalytic properties of the G–C_{60} hybrid were explored. In this context, the as-prepared G–C_{60} was investigated as an electrocatalyst for the HER *via* the performance of LSV measurements in a N_2-saturated aqueous solution 0.1 M KOH electrolyte. The polarization curves of the synthesized G–C_{60}, precursors GF and C_{60}-pyr-NH_2 as well as commercially available Pt/C (20 wt% on carbon black) are illustrated in Fig. 4(A) and summarized in Table S2 in the ESI.† An onset overpotential at −0.562 V *versus* RHE for G–C_{60} was recorded, which was more positive than the ones recorded for the precursors C_{60}-pyr-NH_2 (at −1.488 V) and GF (at −1.613 V), respectively. Concerning the evaluation at −10 mA cm^{-2}, which is the functional current density required for sufficient hydrogen production, the overpotential of G–C_{60} was found to be −0.939 V *versus* RHE, 880 and 914 mV more positive than the recorded ones for C_{60}-pyr-NH_2 and GF, respectively. All of the above observations show that G–C_{60} exhibits much higher electrocatalytic activity for the HER in comparison with the used precursors for its synthesis. The great catalytic performance of the G–C_{60} hybrid in alkaline media is attributed to the synergistic effects between the materials that promote the intermolecular electron transfer from the graphene nanosheets to the electron-accepting fullerenes;[31,32] hence, the negative charge density on the fullerene cages facilitates the proton adsorption step and the overall HER activity.[10,13]

Insight into the HER kinetics was obtained by the Tafel slopes extracted from the LSV curves and the EIS measurements. The Tafel slope value for G–C_{60} was found to be 347 mV dec^{-1}, which was lower in comparison with the ones for pristine materials GF and C_{60}-pyr-NH_2, 438 and 542 mV dec^{-1}, respectively (Fig. 4(B)), indicating the easier HER kinetics for G–C_{60}. The EIS measurements were conducted at −2 mA cm^{-2}, a potential where significant HER current was recorded, and EIS data were fitted to Randles circuit. According to the Nyquist plots, G–C_{60} displayed the lowest charge resistance value (R_{ct} = 73 Ω), while GF and C_{60}-pyr-NH_2 exhibited higher R_{ct} values, 188 and 266 Ω, respectively (Fig. 4(C)). The lower charge transfer resistance for G–C_{60} than those of individual components is attributed to the formed π-network due to the nucleophilic substitution of amino-modified fullerene moieties onto FGs and the concurrent reductive defluorination. The latter result is also an extra indication for the successful covalent grafting of amino-modified fullerene moieties onto FGs.

Additionally, the long-term stability of G–C_{60} was evaluated by durability studies. The LSV polarization curves for the HER of G–C_{60} after 1000, 5000 and 10 000 cycles exhibited gradually improved electrocatalytic activity (Fig. 4(A)). Further confirmation of this unusual behavior for G–C_{60} was received by chronoamperometry measurement, which showed enhanced electrocatalytic performance for G–C_{60} after 52 000 seconds (Fig. 4(D)). The self-improving electrocatalytic activity for materials has been reported in other works as well,[33,34] attributed to the activation of more catalytic sites in the hybrids during cycling.

Concerning the estimation of the electrochemically active surface area (ECSA) for G–C_{60} and its precursors (GF and C_{60}-pyr-NH_2), cyclic voltammograms for the HER for each material were measured in a non-faradaic region at scan rates of 50, 100, 200, 300, 400 and 500 mV s^{-1} (Fig. S6–S8, ESI†). ECSA for G–C_{60} was calculated at 1.4 cm^2, which was higher compared to GF (at 1.0 cm^2) and C_{60}-pyr-NH_2 (at 0.3 cm^2), respectively. These values are in agreement with the electrochemical performances for the HER for each material since the efficient accessibility of the active sites is associated with higher ECSA values.

In summary, we report a non-metal G–C_{60} hybrid material evaluated as an electrocatalyst for proton reduction displaying improved HER electrocatalytic activity compared to the reference materials FGs and C_{60}–pyr-NH_2. The interfacial charge-transfer process between the graphene nanosheets and electron-accepting fullerenes boosted the overall HER activity. This synergistic interaction yielded new active catalytic sites that enhanced the electrocatalytic activity of the material. Notably, the G–C_{60} electrocatalyst exhibits high durability for up to 52 000 seconds. The composition based on light and abundant elements together with the facile one-step synthesis of the hybrid opens new avenues for the efficient covalent integration of carbon allotropes towards the preparation of non-metal all-carbon hybrid materials equipped with electrocatalytic activity.

MO gratefully acknowledges the financial support from the ERC (Consolidator grant 683024 from the Horizon 2020). This work was also supported by the Ministry of Education, Youth and Sports of the Czech Republic (project no. CZ.02.1.01/0.0/0.0/16_019/0000754). Operation of XPS and TEM facilities was partly funded by the Research Infrastructure NanoEnzviCz, supported by the Ministry of Education, Youth and Sports of the Czech Republic (project no. LM2018124). We thank J. Havláková for TGA, M. Petr for XPS and K. Štymplová for Raman spectra measurements.

Conflicts of interest

There are no conflicts to declare.

References

1 X. Liu and L. Dai, *Nat. Rev. Mater.*, 2016, **1**, 1–12.
2 Y. Lee, J. Suntivich, K. J. May, E. E. Perry and Y. Shao-Horn, *J. Phys. Chem. Lett.*, 2012, **3**, 399–404.
3 J. Shi, F. Qiu, W. Yuan, M. Guo and Z.-H. Lu, *Chem. Eng. J.*, 2021, **403**, 126312.
4 R. Paul, L. Zhu, H. Chen, J. Qu and L. Dai, *Adv. Mater.*, 2019, **31**, 1806403.
5 I. K. Sideri and N. Tagmatarchis, *Chem. – Eur. J.*, 2020, **26**, 15397–15415.
6 C. Hu, Q. Dai and L. Dai, *Cell Rep. Phys. Sci.*, 2021, **2**, 100328.
7 W. Zhou, J. Jia, J. Lu, L. Yang, D. Hou, G. Li and S. Chen, *Nano Energy*, 2016, **28**, 29–43.
8 A. Kagkoura, R. Arenal and N. Tagmatarchis, *Adv. Funct. Mater.*, 2021, **31**, 2105287.
9 Z. W. Seh, J. Kibsgaard, C. F. Dickens, I. Chorkendorff, J. K. Nørskov and T. F. Jaramillo, *Science*, 2017, **355**, eaad4998.
10 M. A. Ahsan, T. He, K. Eid, A. M. Abdullah, M. L. Curry, A. Du, A. R. Puente Santiago, L. Echegoyen and J. C. Noveron, *J. Am. Chem. Soc.*, 2021, **143**, 1203–1215.
11 M. Chen, R. Guan and S. Yang, *Adv. Sci.*, 2019, **6**, 1800941.
12 A. R. Puente Santiago, O. Fernandez-Delgado, A. Gomez, M. A. Ahsan and L. Echegoyen, *Angew. Chem., Int. Ed.*, 2021, **60**, 122–141.
13 R. Gao, Q. Dai, F. Du, D. Yan and L. Dai, *J. Am. Chem. Soc.*, 2019, **141**, 11658–11666.
14 Z. Du, N. Jannatun, D. Yu, J. Ren, W. Huang and X. Lu, *Nanoscale*, 2018, **10**, 23070–23079.
15 J. Guan, X. Chen, T. Wei, F. Liu, S. Wang, Q. Yang, Y. Lu and S. Yang, *J. Mater. Chem. A*, 2015, **3**, 4139–4146.
16 A. Hasanzadeh, A. Khataee, M. Zarei and Y. Zhang, *Sci. Rep.*, 2019, **9**, 13780.
17 D. D. Chronopoulos, A. Bakandritsos, M. Pykal, R. Zbořil and M. Otyepka, *Appl. Mater. Today*, 2017, **9**, 60–70.
18 X. Chen, K. Fan, Y. Liu, Y. Li, X. Liu, W. Feng and X. Wang, *Adv. Mater.*, 2022, **34**, 2101665.
19 D. D. Chronopoulos, M. Medved', P. Błoński, Z. Nováček, P. Jakubec, O. Tomanec, A. Bakandritsos, V. Novotná, R. Zbořil and M. Otyepka, *Chem. Commun.*, 2019, **55**, 1088–1091.
20 A. Bakandritsos, M. Pykal, P. Błoński, P. Jakubec, D. D. Chronopoulos, K. Poláková, V. Georgakilas, K. Čépe, O. Tomanec, V. Ranc, A. B. Bourlinos, R. Zbořil and M. Otyepka, *ACS Nano*, 2017, **11**, 2982–2991.
21 F. Huang, Y. Li, X. Liu, W. Lai, K. Fan, X. Liu and X. Wang, *Chem. Commun.*, 2021, **57**, 351–354.
22 Y. Zhang, M. Melchionna, M. Medved, P. Błoński, T. Steklý, A. Bakandritsos, Š. Kment, R. Zbořil, M. Otyepka, P. Fornaserio and A. Naldoni, *ChemCatChem*, 2021, **13**, 4372–4383.
23 M. F. Sanad, V. S. N. Chava, A. E. Shalan, L. G. Enriquez, T. Zheng, S. Pilla and S. T. Sreenivasan, *ACS Appl. Mater. Interfaces*, 2021, **13**, 40731–40741.
24 K. Kordatos, T. Da Ros, S. Bosi, E. Vázquez, M. Bergamin, C. Cusan, F. Pellarini, V. Tomberli, B. Baiti, D. Pantarotto, V. Georgakilas, G. Spalluto and M. Prato, *J. Org. Chem.*, 2001, **66**, 4915–4920.
25 K. E. Whitener, R. Stine, J. T. Robinson and P. E. Sheehan, *J. Phys. Chem. C*, 2015, **119**, 10507–10512.
26 D. García, L. Rodríguez-Pérez, M. A. Herranz, D. Peña, E. Guitián, S. Bailey, Q. Al-Galiby, M. Noori, C. J. Lambert, D. Pérez and N. Martín, *Chem. Commun.*, 2016, **52**, 6677–6680.
27 A. B. Bourlinos, K. Safarova, K. Siskova and R. Zbořil, *Carbon*, 2012, **50**, 1425–1428.
28 A. Kouloumpis, D. D. Chronopoulos, G. Potsi, M. Pykal, J. Vlček, M. Scheibe and M. Otyepka, *Chem. – Eur. J.*, 2020, **26**, 6518–6524.
29 J. T. Robinson, J. S. Burgess, C. E. Junkermeier, S. C. Badescu, T. L. Reinecke, F. K. Perkins, M. K. Zalalutdniov, J. W. Baldwin, J. C. Culbertson, P. E. Sheehan and E. S. Snow, *Nano Lett.*, 2010, **10**, 3001–3005.
30 M. Maggini, G. Scorrano and M. Prato, *J. Am. Chem. Soc.*, 1993, **115**, 9798–9799.
31 M. Barrejón, M. Vizuete, M. J. Gómez-Escalonilla, J. L. G. Fierro, I. Berlanga, F. Zamora, G. Abellán, P. Atienzar, J.-F. Nierengarten, H. García and F. Langa, *Chem. Commun.*, 2014, **50**, 9053–9055.
32 M. R. Cerón, C. Zhan, P. G. Campbell, M. C. Freyman, C. Santoyo, L. Echegoyen, B. C. Wood, J. Biener, T. A. Pham and M. M. Biener, *ACS Appl. Mater. Interfaces*, 2019, **11**, 28818–28822.
33 M.-R. Gao, J.-X. Liang, Y.-R. Zheng, Y.-F. Xu, J. Jiang, Q. Gao, J. Li and S.-H. Yu, *Nat. Commun.*, 2015, **6**, 5982.
34 M. Aygün, M. Guillen-Soler, J. M. Vila-Fungueiriño, A. Kurtoglu, T. W. Chamberlain, A. N. Khlobystov and M. Carmen Gimenez-Lopez, *ChemSusChem*, 2021, **14**, 4973–4984.